Journal of Hazardous Materials, 11 (1985) 91—124
Elsevier Science Publishers B.V., Amsterdam — Printed in The Netherlands

THORNEY ISLAND: ITS GEOGRAPHY AND METEOROLOGY

M.E. DAVIES and S. SINGH

Applied Fluid Mechanics Division, NMI Ltd., Teddington, Middlesex (Great Britain)*

(Received December 22, 1984; accepted January 2, 1985)

Summary

A general description of the Thorney Island site is given together with a summary of its prevailing weather conditions.

The specific aspects of surface roughness measurement and atmospheric stability classification are given detailed attention.

As an illustration of the use of the environmental sensor data, four trials are studied covering a range of conditions from highly unstable through neutral to stable atmospheres. The difficulties in deriving an "unanimous" verdict on atmospheric stability class are addressed.

1. Introduction

This paper complements the introductory papers of McQuaid [1], Johnson [2] and Leck and Lowe [3]. Its purpose is to set the scene in terms of the environment in which the Heavy Gas Dispersion Trials were conducted. Of primary importance was the characterisation of the surface in physical and aerodynamic terms, together with a full description of the wind in which the cloud was dispersing.

The utilisation of such data varies considerably from one modeller (physical or numerical) to another, so the principle adopted was to measure most basic parameters in a comprehensive manner, such that further properties could be calculated as required by a particular analyst. Clearly the consequence of such a blanket approach is the risk of a rather less discriminating attitude than would be the case when undertaking specific precision meteorological experiments.

Measurements on the occasions of the trials were recorded in a raw fashion so as to allow later analysis, whilst at other times data was routinely collected and processed to provide background statistics to add to earlier historical records.

In later sections some of these overall statistics are presented, together with samples of the more detailed data available for the trials. The purpose in the latter case is to indicate how the information has been treated to provide the summary data distributed with the trials results.

*Now British Maritime Technology Ltd.

0304-3894/85/$03.30

2. Trials site geography

The Thorney Island trials site is a disused airfield chosen for its flatness and practical suitability in terms of services and security. Figure 1 shows the location of the site on the Sussex coast of Southern England. The island covers an area of around 7 square kilometers and the trials were conducted at the southern end. Figure 2 shows an aerial view of the area. The main runways point approximately to the South and South-West in a seaward direction. Beyond the airfield the fetch in the prevailing wind direction between the two runways comprises 3 km of sheltered water bounded by the low lying tip of Hayling Island beyond which is the English Channel. The airfield itself is relatively uniform and flat and a distance of 1 km of grass and runway lies upwind of the spill point. The spill point can be seen in Fig. 2 to the left of the runway intersection. The figure also shows the area of the runway that was painted white to minimise the temperature differential between the grass and the runway surface. The grass on the site was cut periodically to obtain some measure of consistency of surface condition. Typically, as seen in Fig. 3, the grass had a height of around 20 cm (compare with gas sensor at 0.4 m in Fig. 3). At the outset of the project it was assessed that this would result in an aerodynamic roughness height (z_0) of around 20 mm and this was in accordance with standard references such as the ESDU data sheets [9] (Fig. 4). An assess-

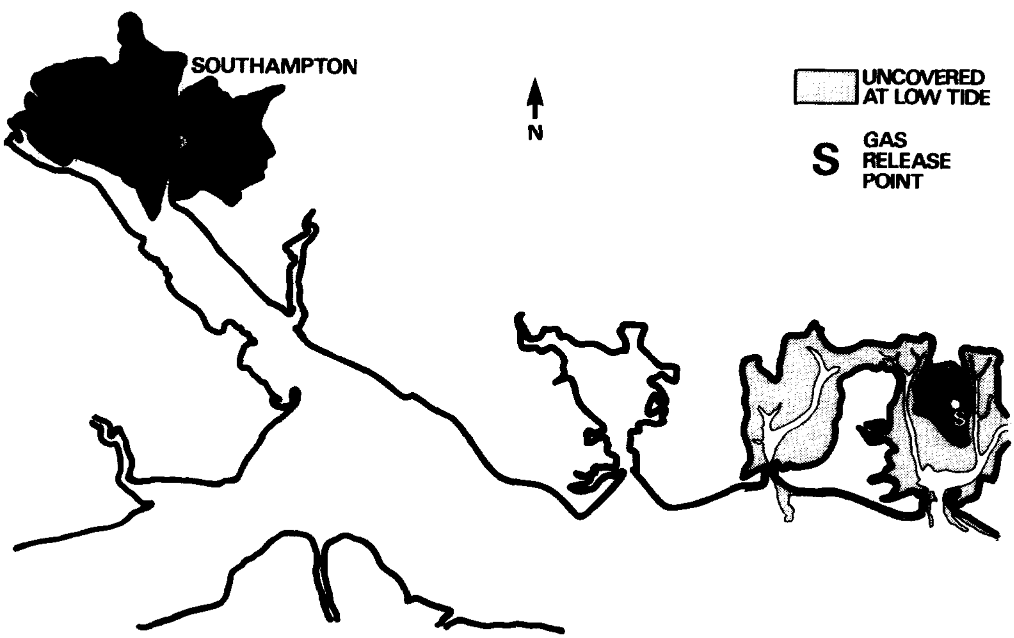

Fig. 1. Location of trials site at Thorney Island.

ment of the value z_0 from subsequent measurements is presented later in Section 4.1.

After careful consideration of the optimum location of the spill point and a suitable array of measurement masts the choice produced a centre-line to the spill point along the compass direction 207°, that is a heading 27° west of south. The mast positions are given in McQuaid [1] and in the main were at the nodes of the grid of 100 m squares shown in Fig. 5. Figure 5 is a contour map of the terrain downwind of the spill point to the extremities of the measurement stations which are at 750 m on the centre-line and at ± 300 m on the flanks. Relative to the spill point elevation much of the field is within ±0.5 m, but there is a gradual fall of the ground beyond 400 to 500 m to a lowest level of −2.5 m. On average the site slope was of order 0.2° and was generally within 0.1° in the first 500 m downwind of the spill point.

Fig. 2a. Aerial view of trials site.

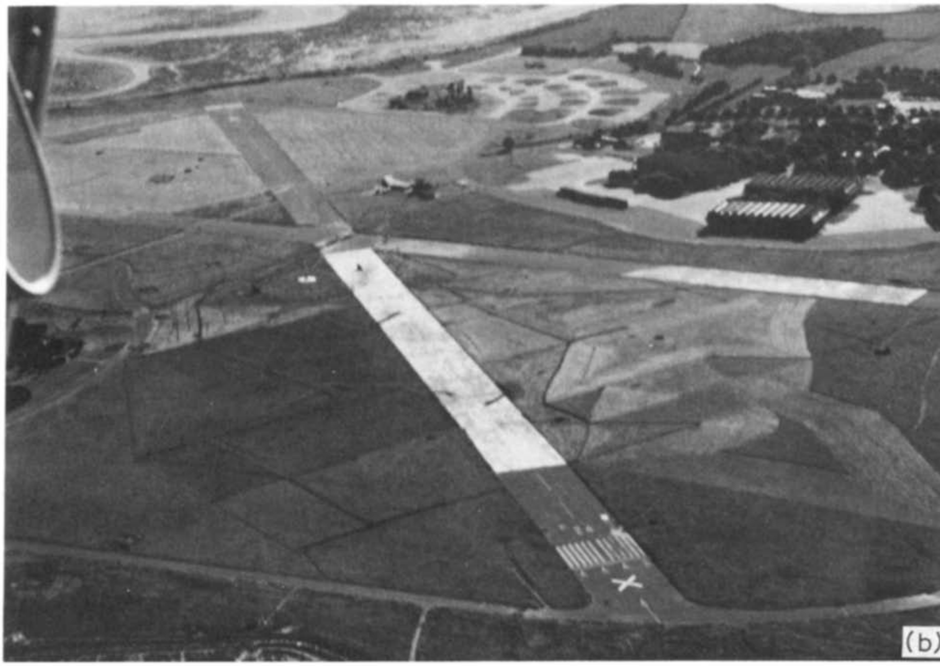

Fig. 2b. Aerial view of trials site.

3. Historical meteorological data

A significant advantage attendant to the availability of Thorney Island as the trials site was its rich history of meteorological records and analysis (e.g. Watts [10]). Fortunately also it became possible to obtain helpful advice from the Meteorological Office at Southampton from forecasters who had previously served on Thorney Island airfield. Certain standard meteorological data existed for periods spanning 1950 to 1975 and this was examined at the planning stage of the trials. Figure 6 is a cumulative distribution of wind speeds from all directions which showed that for about 65% of the time winds in the range of 1.5 m/s to 9 m/s could be expected. Within this speed range, the distribution with direction (Fig. 7) showed a prevailing bearing around 240° and an annual probability of around 20% for occurrence in the range of 160° to 250°. This range suited trials based on the array layout described in Section 2 and a centre-line along 207°.

In order to obtain further information on the best time of the year and the most appropriate time of day to conduct trials, data for the period 1959 to 1975 were analysed. The results of these analyses were presented for each month of the year (e.g. Table 1) to show the number of occurrences (based on the average over 17 years of observations) of winds of bearings in the range 207 ± 45° for various wind speeds and for each hour of

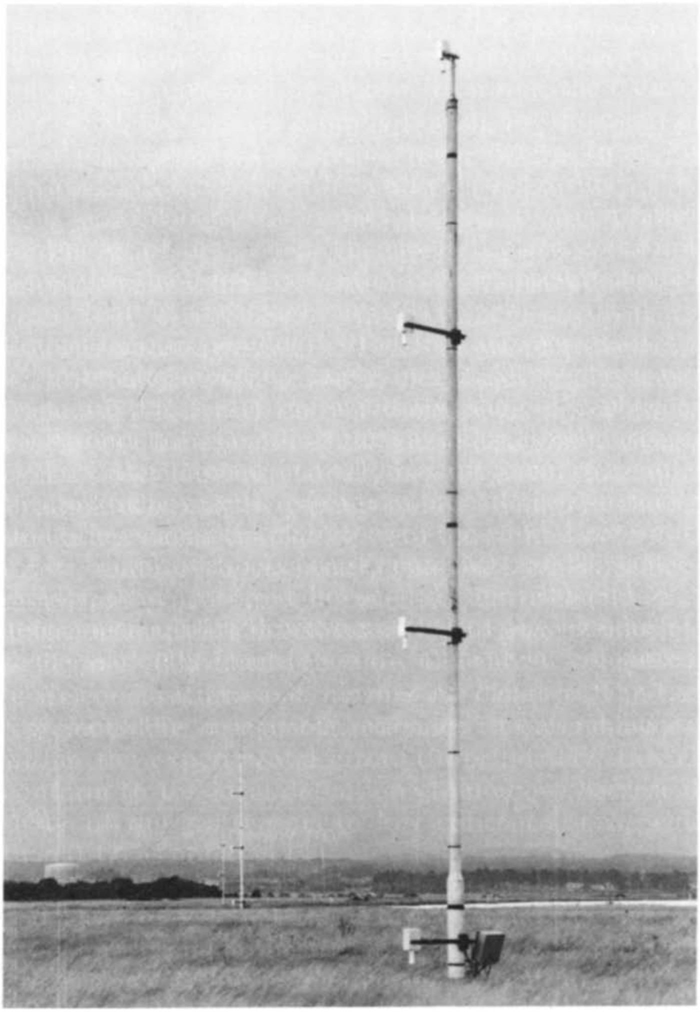

Fig. 3. Measurement station in typical grass area (lowest gas sensor at 0.4 m).

the day. These results showed that favourable conditions were more likely to exist during the period of late spring, through summer to early autumn, with July appearing likely to be the best month. In addition, it was also apparent that the highest probability of favourable winds would be during daylight hours in these months. At other times it was evident that the number of occurrences were fewer and were equally likely to occur at anytime during the 24 hour period.

Wind speed and direction were not, of course, the only parameters used in defining the appropriate trials environment. At the outset it was planned that the trials should include at least five different initial conditions and

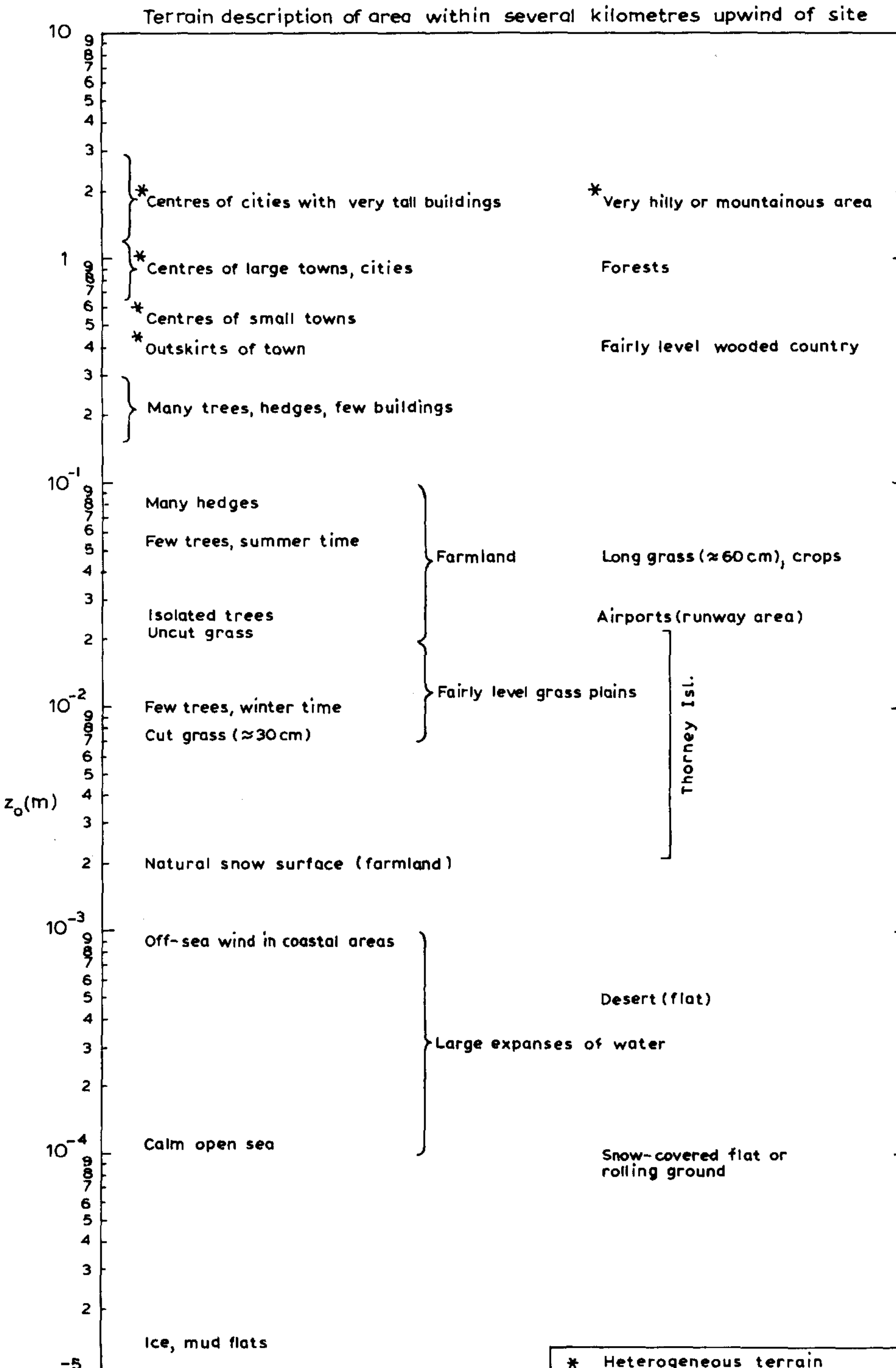

Fig. 4. Estimation of roughness length from ESDU [9].

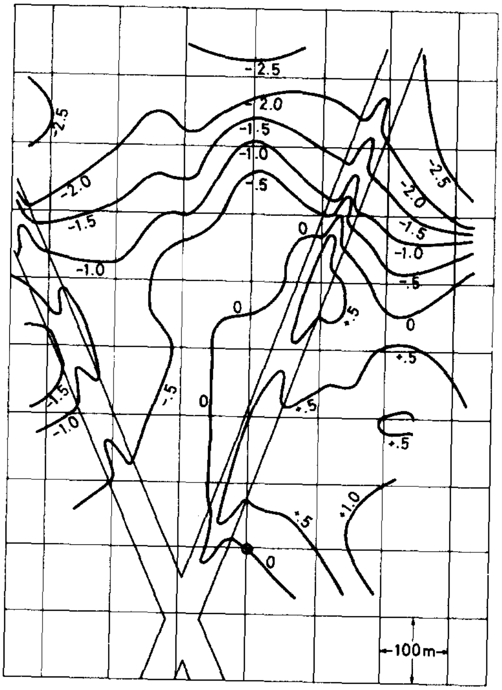

Fig. 5. Thorney Island surface contours; elevation (m) relative to spill point.

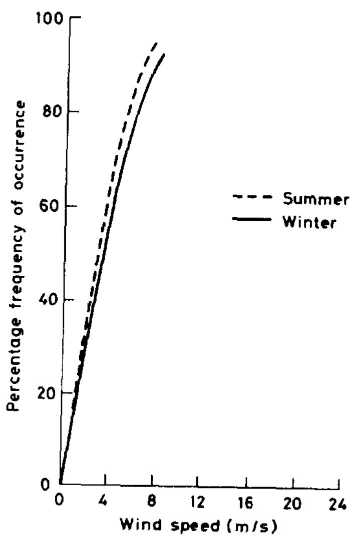

Fig. 6. Frequency of occurrence of winds less than a given speed (data: 1950—1959, all directions, hourly means).

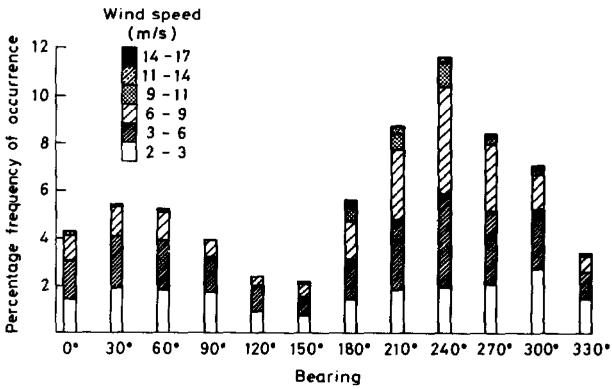

Fig. 7. Annual distribution of winds at Thorney Island (data as in Fig. 6; calms (<1.5 m/s) 29.9%).

TABLE 1

Number of occurrences of winds in the direction ±45° of the array centre line for the month of July at Thorney Island (based on the average of observations over 17 years from 1959—1975)

Time of day	Wind speed bands					
	Calm	1—3 kts (0.5—1.5 m/s)	4—6 kts (2—3 m/s)	7—10 kts (3.5—5 m/s)	11—16 kts (5.5—8 m/s)	17—98 kts (8.5—49 m/s)
0	3.2	1.1	1.3	1.8	2.6	0.8
	3.8	1.2	1.1	1.9	2.6	0.6
2	3.2	1.0	0.6	1.9	2.5	0.6
	3.9	0.8	1.1	1.5	2.9	0.5
4	3.5	0.8	0.7	1.8	2.9	0.4
	3.9	0.4	0.6	1.8	2.9	0.3
6	3.0	0.6	0.7	1.8	2.8	0.5
	1.7	0.5	0.8	1.6	2.9	0.8
8	1.4	1.7	0.8	2.1	3.6	0.9
	0.5	2.2	1.7	3.4	3.6	1.1
10	0.5	1.6	2.5	4.1	4.5	1.3
	0.2	1.2	2.4	5.8	5.1	1.8
12	0.1	0.5	1.8	7.2	6.8	1.9
	0.1	0.8	1.0	6.8	7.8	2.9
14	0	0.5	1.7	7.2	7.9	2.9
	0.2	0.5	2.1	6.8	8.2	3.0
16	0	0.6	1.9	6.6	7.9	2.9
	0.2	0.8	2.4	6.6	6.6	2.8
18	0.2	1.0	2.9	6.2	6.6	1.8
	0.3	2.9	2.7	4.9	5.6	1.4
20	1.4	2.0	2.1	4.3	4.3	0.8
	2.1	1.7	2.5	3.4	2.8	0.8
22	2.6	1.7	1.3	2.4	2.7	0.9
	2.8	1.0	1.2	2.1	2.6	0.9
24						

TABLE 2

Selected release conditions;

Pasquill stability condition sub-range	Wind speed sub-range (m/s)			
	0–2	2–4	4–6	6–8
A, B		12	8	
C, D		2, 5, 6	7, 10	3, 15
E, F	1, 9, 14	4, 11, 13		

Notes: Nos. 5 and 13 are neutrally-buoyant releases; No. 14 is at an initial density ratio of 4.2.

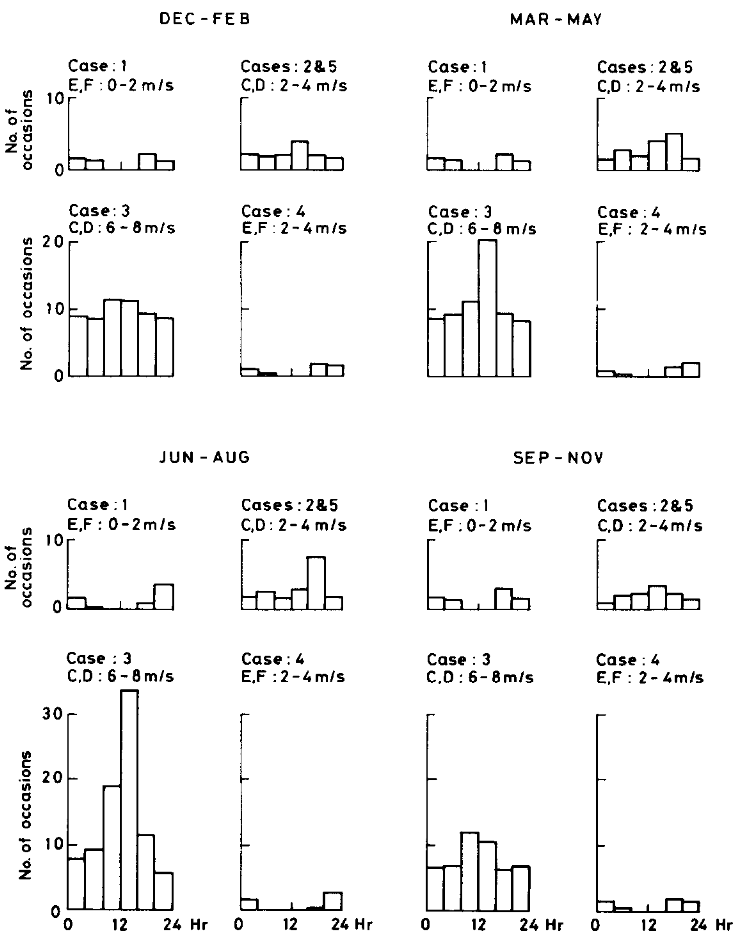

Fig. 8. Likely occurrence of Table 2 conditions from 1959 to 1975 data.

four of these should be different atmospheric conditions (wind speed and stability). These five conditions, together with other desired releases are shown in Table 2.

In order to obtain information on the likelihood of obtaining the atmospheric conditions for the five primary spills of Phase I, the existing data was examined including the extra dimension of atmospheric stability. The results are presented in Fig. 8 and show the number of likely occurrences for each condition during the four seasons of the year. Regardless of the season, it was obvious that the third case was most likely to be achieved; this prescribed wind speeds in the region 6—8 m/s and atmospheric stabilities in the C to D category (according to the Pasquill classification). Of more concern was the fact that the likelihood of obtaining the stable conditions as required for cases 1 and 4 was very low and virtually impossible during daylight hours. The slightly unstable or neutral case with wind speeds in the range 2 m/s to 4 m/s appeared to be a little more likely, with the best chances during the summer between 17.00 and 20.00 hours.

To some extent the probabilities relating to daylight hours are inevitable consequences of the definitions of stability employed in the Meteorological Office for routine data. Table 3 indicates that by definition stable E, F and G categories exist only at night. In reality, however, the thorny issue of atmospheric stability is rather more a question of the degree of "dispersive activity" in the wind and properly becomes a matter of measurement of more fundamental properties of the turbulent planetary boundary layer flow. This subject is returned to in more detail in Section 4.

TABLE 3

Modified Pasquill stability classes (Pasquill [11])

Wind speed (kt)[a]	*Daytime*[b] Incoming solar radiation (W m^{-2})				Within 1 hour before sunset or after sunrise[c]	*Night-time* Cloud amount (oktas)		
	Strong (>600)	Moderate (300—600)	Slight (<300)	Overcast		0—3	4—7	8
⩽3	A	A—B	B	C	D	F or G[d]	F	D
4—5	A—B	B	C	C	D	F	E	D
6—9	B	B—C	C	C	D	E	D	D
10—12	C	C—D	D	D	D	D	D	D
>12	C	D	D	D	D	D	D	D

[a] 1 kt = 0.52 m/s.
[b] Excluding 1 hour after sunrise and 1 hour before sunset.
[c] Night was originally defined to include periods of one hour before sunset and after sunrise. These two hours are always categorised here as D.
[d] Pasquill said that in light winds on clear nights the vertical spread may be less than for category F but excluded such cases because the surface plume is unlikely to have any definable travel. However, they are important from the point of view of the build up of pollution and category G (night-time, 0 or 1 okta of cloud, wind speed 0 or 1 kt) has been added.

4. Measurements to assess site characteristics and atmospheric stability

4.1 Surface roughness

In the absence of detailed measurements surface roughness is commonly judged from an assessment of the physical characteristics of the surface and the obstacles in the path of the wind. Figure 4 was mentioned in Section 2 and the figure serves to illustrate the approximate nature of the description. The roughness length, z_0, is not a measure of a specific physical property of a surface, rather it is a length scale required to characterise the profile of horizontal velocity, U, in the logarithmic "law of the wall" (e.g. Tennekes and Lumley [4]), $U/u_* = (1/k)\ln(z/z_0)$, ($k \approx 0.41$). The friction velocity u_* and roughness length z_0 can be determined directly from the velocity profile (U vs. z) providing a sensible logarithmic region exists.

At Thorney Island the meteorological mast was positioned 150 m upwind of the spill point along the array centre-line (Fig. 5). For the majority of the trials the mast was 30 m high and Porton cup anemometers were deployed at heights of 2 m, 4.5 m, 10 m, 17.3 m and 30 m giving a fairly even spacing on a logarithmic scale (Fig. 9 shows the final 20 m meteorological mast which was utilised for the continuous release trials following severe storm damage to the original). Measurements from these anemometers under conditions of neutral atmospheric stability provided the first method of estimating u_* and z_0.

The obvious direct method of estimating u_* from Reynolds stress measurements was utilised as a second approach to the definition of z_0. In the constant stress region expected in the lower part of the planetary boundary layer measurements of $\overline{u'w'}$ (the correlation of along wind and vertical velocity fluctuations) yield estimates of u_* from the surface relationship $u_*^2 = -\overline{u'w'}$.

Three-component sonic anemometers were mounted on the weather mast at 2 m and 10 m. Potentially the transducers can provide comprehensive estimates of all velocity correlations and heat fluxes at a number of heights, but for the purposes of this paper only measurements from the 10 m location have been analysed. From estimates of u_* from the Reynolds stress $\overline{u'w'}$, z_0 was calculated from the associated logarithmic velocity profile (Tennekes [5]). The 10 m sonic anemometer was also used to provide the normal stresses (the turbulence levels σ_u, σ_v and σ_w) and to allow further estimates of u_* to be made from the r.m.s. along wind and vertical velocities using the proportionality cu_* where c is 2.5 and 1.3 respectively (Lumley and Panofsky [6], Smith [7]).

Looking first at the profile measurements, Figs. 10 and 11 show data collected in 1982. The flagged symbols relate to measurements in the winter prior to the mast's deployment 150 m upwind of the spill point. During this period the weather station was positioned to the west of the control tower but in a similar environment and with a similar fetch from the sea to its final position. The acceptance angle for wind heading was taken to be ±60° of the array centre-line direction. The remaining data in Figs. 10 and 11 appeared to confirm the derived values of u_* and z_0 and this early information was taken as a working assumption for the site. The line in Fig. 10 was a best fit to the data and this was transposed to z_0 in Fig. 11. Generally speaking the measurements made the site appear smoother than anticipated and the figures showed an uncertain trend with increasing wind speed.

To obtain confirmation or otherwise of these results Fig. 12 has been assembled on the basis of the range of estimation procedures described above on measurements different from those in Figs. 10 and 11. For com-

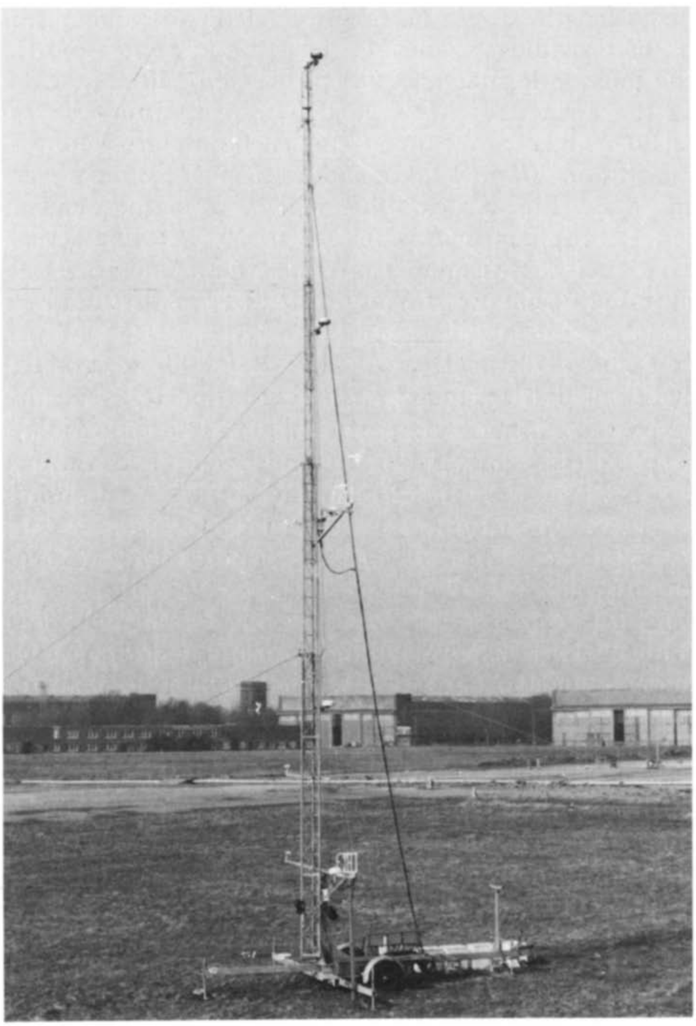

Fig. 9. Final (20 m) meteorological mast used for 'continuous' release trials.

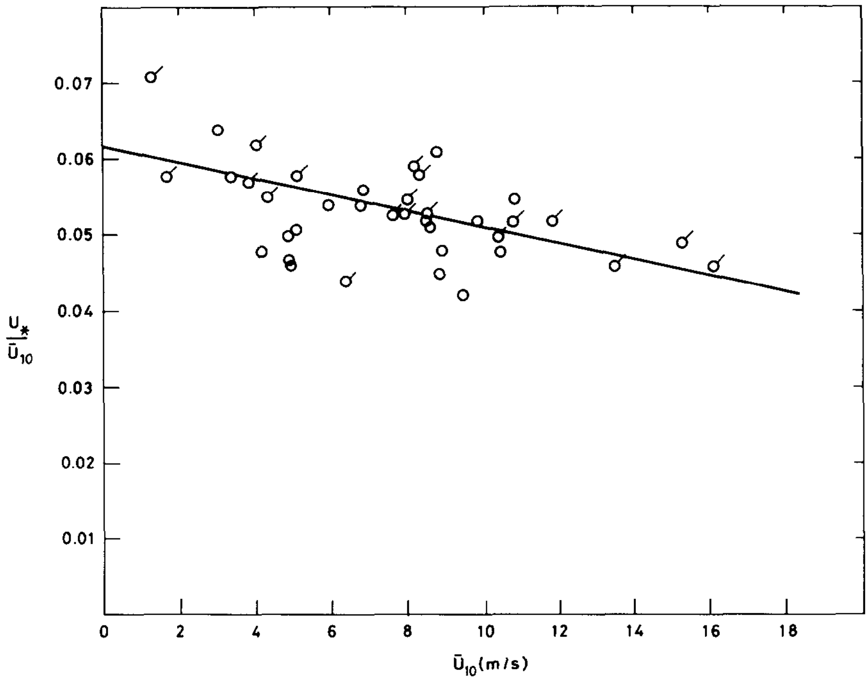

Fig. 10. Friction velocity from profile measurements (1982 data, ○ at final location, ♂ at 'winter' position).

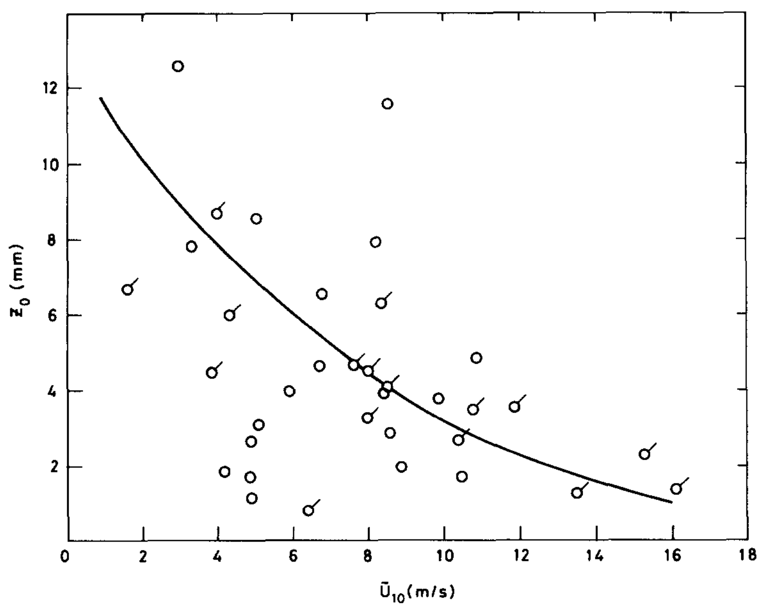

Fig. 11. Roughness length from profile measurements (data as Fig. 10).

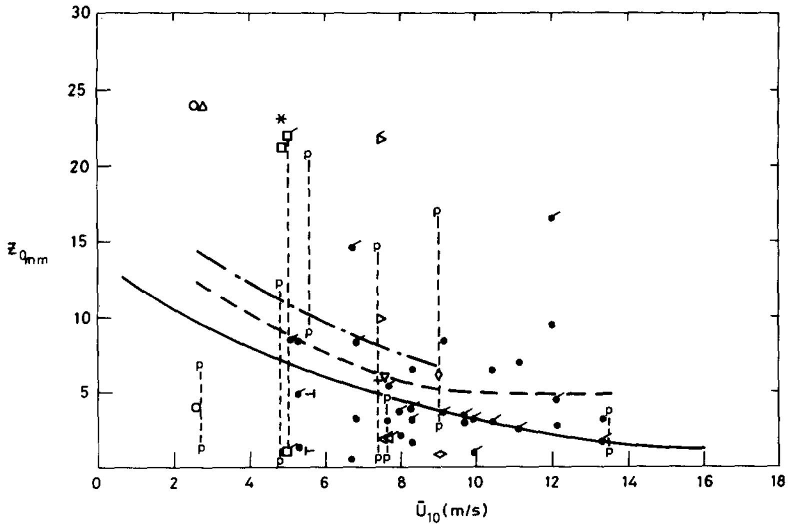

Fig. 12. Roughness length estimates. Key: table below.

Symbol	Trial	Calc. method		
○	006	*uw*		
♂	006	*uw* (Shell)		
△	006	*u'*		
p	006	profile		
◁	013	*uw*		
◁ (flagged)	013	*uw* (Shell)		
▽	013	*u'*		
p	013	profile		
□	016	*uw*		
□ (flagged)	016	*uw* (Shell)		
*	016	*u'*		
p	016	profile		
▷	018	*uw*		
▷ (flagged)	018	*uw* (Shell)		
+	018	*u'*		
p	018	profile		
◇	028	*uw*		
◇	028	*u'*		
p	028	profile		
⊢	029	*uw*		
⊣	029	*u'*		
p	029	profile		
•	Routine data collection	*u'*	1983/4	——— Fig. 11
• (flagged)	Routine data collection	*w'*	1983/4	– – – – average through data — — — from $\overline{uw}$ data only

parison, however, the average z_0 line from Fig. 11 has been redrawn. Estimates from a number of trials are shown together with those from routine data collection runs over 10 minutes which in this case were restricted to winds within ±30° of the array centre-line. The wind directions for the trials analysed are shown in Fig. 13. (This figure also includes 'non-neutral' Trials 004 and 009.)

A range of z_0 values derived from profile measurements averaged over the trial main data segments is shown in Fig. 12. The trial conditions were judged to be neutrally stable and reasonable straight lines could be drawn on logarithmic profile plots, though a range of slopes was possible and these are reflected in the bands shown in Fig. 12. Also plotted are z_0 estimates from a profile measured in a wind speed at 10 m of 13.3 m/s. The wind bearing lay between trials 029 and 013 in Fig. 13. In such high winds there should be no doubt that the boundary layer was neutrally stable and a 'log law'' profile should be evident. Figure 14 confirms the assertion and indicates the relatively small range of u_* and z_0 which may be plausibly derived from this data. It is interesting to note on Fig. 12 that the profile data (cup anemometers) and turbulence measurements (sonic anemometer) yield the same estimates for z_0.

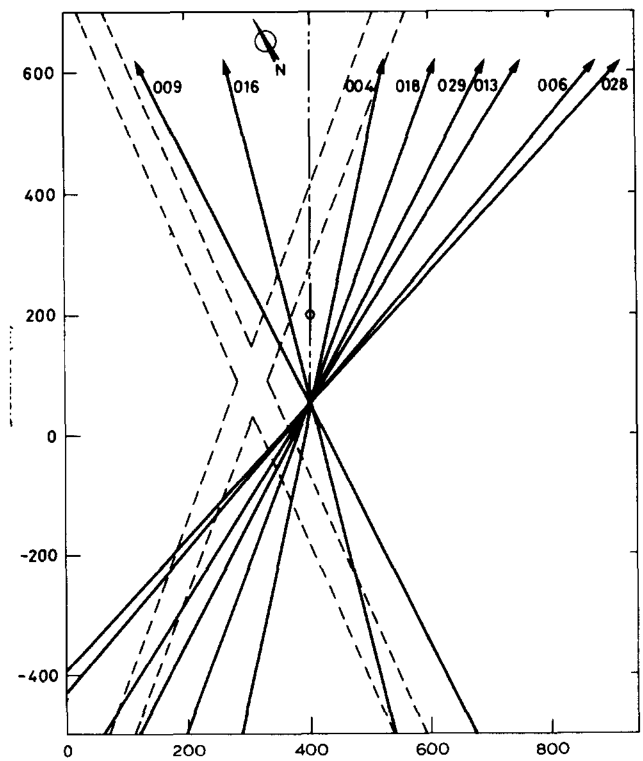

Fig. 13. Mean wind directions for selected trials.

For certain trials two estimates are given utilising Reynolds stress measurements. Those marked 'Shell' have been computed by Puttock and Colenbrander as described in [8] and include a combined "tilt/distortion" correction evaluated from the mean measured vertical velocity. In relation to z_0 no consistent behaviour is evident between corrected and raw estimates.

Overall, Fig. 12 shows a scatter between 1 mm and 25 mm but with a preponderance of estimates close to the original (Fig. 11) line. Taking advantage of all estimates grouped in 2 m/s bands results in the chain line in Fig. 12. This line exhibits the same trend as that from the original profile data, as indeed does the third line which is based on the average of Reynolds stress estimates only.

As this analysis has demonstrated it is hardly surprising that z_0 is rarely known to better than an order of magnitude for many sites. (This analysis of the Thorney Island data places the site conveniently between "off-sea winds in coastal areas" and "airports" in Fig. 4.) Roughness length is an inherently sensitive parameter and whether there is any variation with wind speed is largely an academic question in practice. Whilst on the basis of a long homogeneous upwind fetch and a constant physical roughness no change should exist, it is possible that 'compliant' long grass and short upwind distances to roughness changes (e.g. runways, Fig. 13) may have led to a genuine dependence on wind speed.

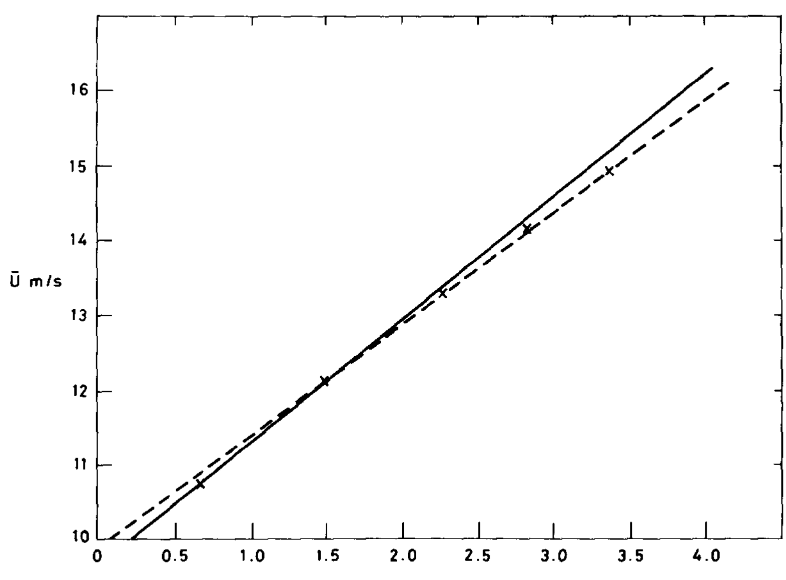

Fig. 14. Logarithmic velocity profile in high winds (U_{10} = 13.3 m/s, $\bar{\theta}$ = +28°).

4.2 Atmospheric stability categorisation

Beyond the stage of gravity dominated dense cloud spreading, all models require to represent the mixing potential of the atmospheric wind. For many applications the details of the turbulent boundary layer are not known and recourse has to be made to simple categorisations of atmospheric conditions to broadly classify the boundary layer's dispersive properties. To this end Pasquill's stability classes [11] were devised and can be conveniently assessed from routine meteorological measurements as we have seen in Table 3. However, although plume dispersion predictions based on these schemes have stood modellers in good stead over many years, the approximate nature of such descriptions of the atmosphere should be recognised.

In Pasquill's words: "The system of stability categories defined in terms of routine meteorological data . . . was originally introduced as a practical substitute for measurements of turbulence. The latter measurements would provide a much more direct and reliable indication of dispersion . . ."; and in 1981 a diffusion workshop report [12] stated: "The workshop results de-emphasize relying on Pasquill—Gifford—Turner (PGT) stability classification as a primary means of characterizing atmospheric diffusion; rather, they emphasize relying upon on-site measurements of turbulence intensity to characterize the dispersion properties of the atmosphere. This is a major step forward from the assumptions of many models currently used in air pollution control evaluation".

This advice was restated by the Meteorological Office at an early stage of the project and in general it is expected that the analysts of the Thorney Island trials will use the most relevant turbulence measurements for purposes of validation and development of models. In spite of this expectation and to some extent because of the range of measured parameters, there remains an interest in trying to reconcile detailed boundary layer measurements with the simple Pasquill categories.

The last decade or so has seen considerable effort in this direction and examples of this work appear in Golder [13], US NRC [14], Smith [15], Sedefian and Bennett [16] and Tagliazucca and Nanni [17]. As a matter of routine the schemes of Sedefian and Bennett were employed to classify the atmospheric stability as measurements were made on the site and subsequently some additional processing was undertaken to amplify the results. The remainder of this Section is devoted to outlining the classification methods used and Section 5 provides examples of their use on particular trials.

4.2.1 Observation (basic Pasquill method)

(U_{10}, insolation (R) (estimate)/cloud cover)

The method requires a measurement of wind speed at 10 m and a judgement of cloud cover or insolation. The stability class can then be judged from Table 3, which is appropriate to the UK. Strong insolation refers to a sunny mid-summer's day.

4.2.2 *Insolation measurement*

<u>(U_{10}, R)</u>

In this refinement of 4.2.1, the incoming solar radiation was measured by a solarimeter at 0.4 m above the ground and the estimate of stability was made from Fig. 15. If it is assumed that u_* is a velocity scale that removes the dependence on roughness length then the wind speed values at 10 m on Fig. 15 should be increased by about 50% for Thorney Island.

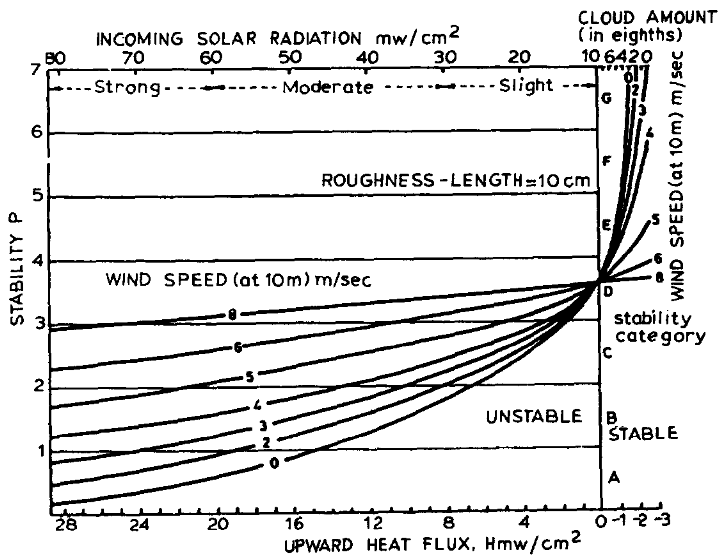

Fig. 15. Stability as a function of heat flux and wind speed (from Pasquill [11]).

4.2.3 *Heat flux estimates*

<u>(R, U_{10}, u_*, $w(t)$, $T(t)$)</u>

A number of estimates of heat flux can be attained from the basic measurements which are available and the Monin—Obukhov and Kazanski—Monin stability parameters are then readily derived.

<u>$H_1 = 0.4\,(R - 100)$ (W/m²) (Smith [15])</u>

This approximate empirical formulation was derived by Smith for unstable conditions. Essentially the "top" and "bottom" scales in Fig. 15

are related in this way and generally the stability categories derived from this method and 4.2.2 will be identical. Inspection of Fig. 15 on the stable side, however, indicates a somewhat different relationship.

$H_2 = C_p\, \rho(\overline{wT} - \overline{w}\,\overline{T})$ (W/m²)

Estimates of heat flux were available directly from the covariance of the fluctuating vertical velocity and temperature. Much has been written on the difficulty of using sonic anemometers for temperature measurement and the Meteorological Office had confirmed this aspect [18]. Although the alternative of a long thin platinum wire mounted in association with the sonic anemometer was employed on the site, this temperature measurement was not consistently available, so the anemometer temperature channel was used in most circumstances.

Kaimal [19] has identified the two sources of error affecting temperature measurement. The first involves the humidity flux, which may or may not be significant on a coastal site. Whilst Kaimal claims that the resulting error in heat flux is not larger than 10% in a case of strong evaporation, Puttock and Colenbrander [8] argue that, in any case, buoyancy flux is more appropriate for stability categorisation and therefore the humidity flux 'error' is best consolidated into the estimate. The second error in temperature is concerned with contamination by the horizontal velocity component, u, and results in a modification to the heat flux estimate of $-2\overline{T}\,\bar{u}\,\overline{uw}/C^2$ ([19], [8]). For the highest wind speeds utilised for trials in the HGDT programme (around 8 m/s) this correction amounts to about 10 W/m².

Results are presented in Section 5 for both corrected and uncorrected heat flux (including humidity flux) measurements.

H_3 from surface energy balance (Jiemin [20] and [21])

This method stems from recent work at the Meteorological Office. The surface energy balance describes the partitioning of incoming net radiation (R_n) into the sensible heat flux (H), the latent heat flux (LE) and the downward flux of heat into the soil (G). The fluxes are estimated by a 'resistance' method based on the electrical analogy, flux = potential difference/resistance. The sensible heat flux H is expressed as

$$H = \Delta T \rho C_p / r_h$$

where r_h is the heat flux resistance and can be written as a function of the integrated similarity function ψ_H.

Routine meteorological data would not normally provide a surface temperature and this method yields estimates through two further resistances — stomatal (r_{st}) and climatological (r_i). These respectively relate to surface evaporation from leaf surfaces and the humidity of the surface layer

$$H_3 = (r_h + r_{st} - r_i)(R_n - G)/(1 + \bar{\Delta}/\gamma)r_h + r_{st}$$

where $\bar{\Delta}$ is a function of the saturated water vapour pressure gradient with temperature and γ is a slowly varying function of temperature.

H_4 from surface energy balance (Holstag and van Ulden [22])

A second method of estimating H from the surface energy balance is provided by Holstag and van Ulden at the Netherlands Meteorological Office Institute. The principles are those of the previous section but different detailed approaches are used to determine the energy partitioning. Resistance estimates are avoided by a simplification due to de Bruin and Holstag [23] which provides the following expression for the sensible heat flux

$$H_4 = ((1 - \alpha) + (\gamma/s))(R_n - G)/(1 + \gamma/s) - \beta$$

α and β are empirical parameters and γ/s is a known function of temperature. In applying this method to the Thorney Island data, empirical coefficients for grass surfaces were used and the on-site measurements of incoming solar radiation were employed in the calculation for R_n, the net radiation.

L, Monin—Obukhov stability length

The Monin—Obukhov length, L, is usually defined as

$$L = -\rho C_p T u_*^3/gkH$$

where ρ is the density of air at temperature T, C_p is the specific heat at constant pressure, u_* is the friction velocity, g is the acceleration due to gravity, k is von Karman's constant (0.4) and H is the sensible heat flux. In the calculation of L the various foregoing heat flux estimates were used and in the case of sonic anemometer measurements H, in both the measurement and in the definition of L, can be considered to include a humidity flux term [8]. The friction velocity, u_*, in the calculations was taken as a fraction of the measured wind speed at 10 metres using Fig. 10.

It has been observed by Readings et al. [18] that the Monin—Obukhov length and the Pasquill stability classes correlate rather poorly, but, nonetheless, estimates of stability class from L can be made from Golder [13] (reproduced as Fig. 16).

μ, Kazanski—Monin stability parameter

Smith [15] has shown that Kazanski and Monin's μ correlates well with Pasquill stability, at least for unstable conditions. μ is a ratio of temperature and momentum flux defined as

$\mu = -gk^2H/fC_pT\rho u_*^2$

where f, the Coriolis parameter, is a function of latitude.

The remarks made in the previous paragraph in relation to H and u_* apply equally to the calculation of μ.

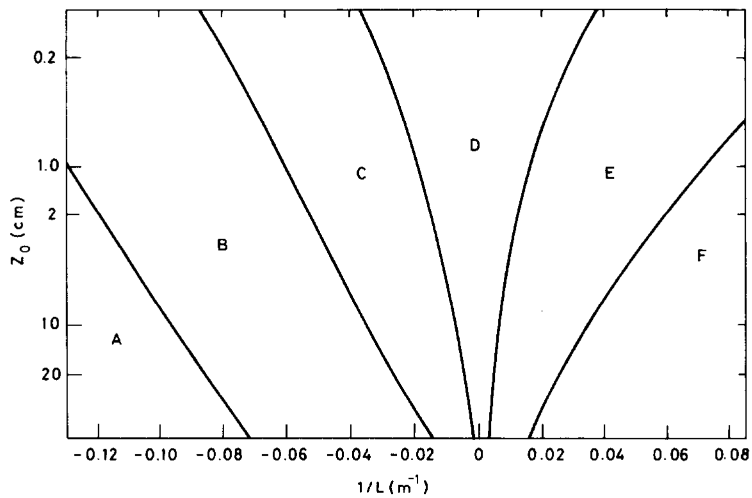

Fig. 16. Stability class as a function of Monin—Obukhov length (L) and roughness z_0 (from Golder [13]).

4.2.4 Temperature gradient (US NRC [14])

<u>(temperature profile)</u>

The US NRC scheme for classification by temperature gradient is presented in Fig. 17. There has been some debate as to the appropriate range over which the gradient should be calculated. Readings et al. [18] specifically highlight the point that the scheme requires temperature gradients from 10 metres to 40 metres or above. At Thorney Island the difference between the 9 m and 30 m sensors was used. Other workers have argued that the lowest sensors should be used. It would appear that two separate points are at issue. The first relates to the "correlation table" used to infer Pasquill stability and clearly temperature gradients in different height ranges may lead to differing correlation patterns. The second and more fundamental point addresses the question of which part of the atmospheric boundary layer is most important for dispersing a low lying heavy gas cloud.

For the purposes of this paper the view has been taken that the most commonly used scheme should be used, since a challenge of this crude correlation between two rather unsophisticated measures of stability is a rather inappropriate basis for a discussion of atmospheric boundary layer physics. Generally the accuracy obtained for the temperature measurements (Johnson [24]) was not sufficient to resolve the finest stability class differentiation on the unstable side and as will be seen in Section 5 a number of consideratiohs lead to uncertainties in the interpretation of the temperature profiles.

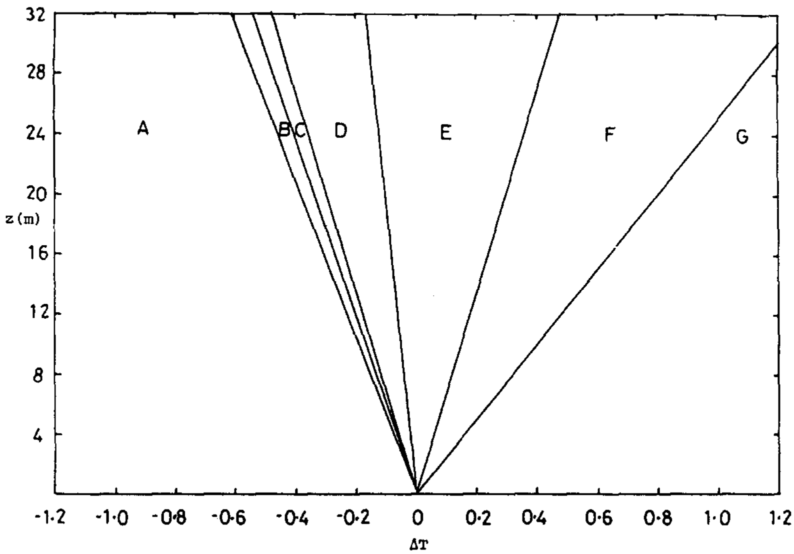

Fig. 17. Stability as a function of temperature gradient (from US NRC [14]).

4.2.5 Gradient Richardson number

(temperature profile, velocity profile)

Following Sedefian and Bennett [16] the gradient Richardson number may be defined as

$$Ri = g(\mathrm{d}\theta/\mathrm{d}z)\,(\mathrm{d}\overline{U}/\mathrm{d}z)^2/T$$

where θ is the potential temperature.

Introducing the usual profile similarity functions for heat and momentum (Dyer [25]) allows Ri to be written as

$$Ri = (z/L)\,(\phi_h/\phi_m^2)$$

where ϕ_h and ϕ_m are functions of the stability scaled height variable (z/L).

From Golder's curves (Fig. 16) the Pasquill stability classes may be expressed in terms of $1/L$ for a given z_0 and hence the equivalent Richardson number limits may be derived for a particular value of z. The appropriate choice of z is the geometric mean height $(z_1 z_2)^{0.5}$ where z_1 and z_2 are the heights between which the temperature and velocity gradients are calculated. Figure 18 displays the relationship between Ri and stability class as a function of z_0 for a height $z = 16$ m, which is close to the geometric mean of z_1 and z_2 which equalled 9 m and 30 m respectively.

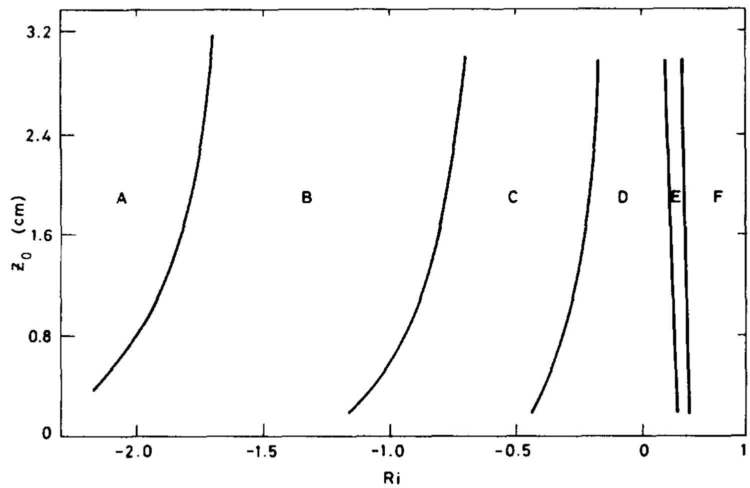

Fig. 18. Stability as a function of gradient Richardson number and roughness length.

4.2.6 *Bulk Richardson number*

(temperature profile, $\bar{U}_{30}$)

A variant of the gradient Richardson number which reduces sensitivity to an uncertain velocity profile is the bulk Richardson number, Ri_B.

$$Ri_B = [g(d\theta/dz)\bar{z}^2]/T\,\bar{U}^2 \qquad [16]$$

where $\bar{z}$ is the geometric mean height as in Section 4.2.5 and $\bar{U}$ is an upper level velocity ($\bar{U}_{30}$ at Thorney Island). In a similar fashion to that for the gradient Richardson number formulation the introduction of the similarity profile functions leads to the expression of Ri_B in terms of the height scaled by the Monin—Obukhov length and thence to the relationship between Ri_B and Pasquill stability shown in Fig. 19.

4.2.7 *Standard deviation of horizontal wind direction*

(US NRC [14])

Table 4 presents Sedefian and Bennett's [16] statement of the US NRC correlation between horizontal wind direction fluctuation and Pasquill stability. σ_θ at $z = 10$ m was available in an approximate way from the

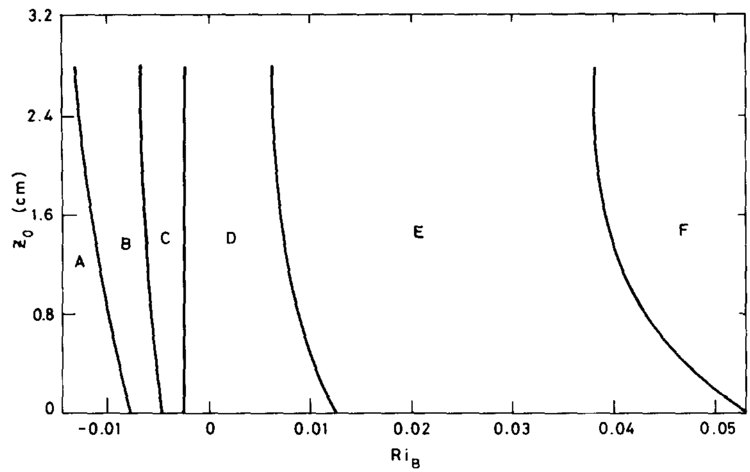

Fig. 19. Stability as a function of bulk Richardson number and roughness length.

TABLE 4

σ_θ as an indicator of Pasquill stability (US NRC limits)

Pasquill class	σ_θ(°)
G	<2
F	>2, <3.75
E	>3.75, <7.5
D	>7.5, <12.5
C	>12.5, <17.5
B	>17.5, <22.5
A	>22.5

Porton wind vane and perhaps more reliably from the sonic anemometer.

In spite of the resolution bandwidth of 11° for the vane, it was possible to demonstrate by numerical simulation (based on normal distributions) that σ_θ should rarely deviate from the true value by more than a degree or so. As we shall see in Section 5, the values obtained from the vane were generally in close agreement with sonic anemometer estimates calculated as $\sigma_\theta = \sigma_v/\overline{U}_{10}$.

5. Environmental measurements for particular trials

To illustrate the application of the stability categorisation schemes and the implications of the surface roughness estimates data from a number of trials will next be considered. Specifically, four trials have been selected to span a range of stability conditions. The trial stability is ultimately a matter of judgement and the reader is, of course, free to draw his own conclusions. Although recipients of trials data have received this judgement as part of the description of the trial, all the basic data exists for any further analysis.

5.1 Turbulence intensity

To place the selected trials in some perspective the turbulence intensity components for all Phase I trials are shown in Fig. 20. The horizontal band for each component is taken from the ESDU data sheets [9] and represents turbulence intensity over terrain with z_0 in the range 2 mm to 20 mm and in neutrally stable conditions. In Fig. 20(b) the additional symbols are estimates of σ_v from σ_θ measurements using the Porton wind vane.

Considering the turbulence measurements relative to the ESDU data gives the following qualitative statements for Trials 004, 006, 009 and 013.

Trial	σ_u	σ_v	σ_w
004	neutral	unstable	unstable
006	neutral/unstable	unstable	unstable
009	stable	neutral	stable
013	neutral	neutral/unstable	neutral

The observations shown are not completely consistent but the ranking of the trials from each criterion is similar.

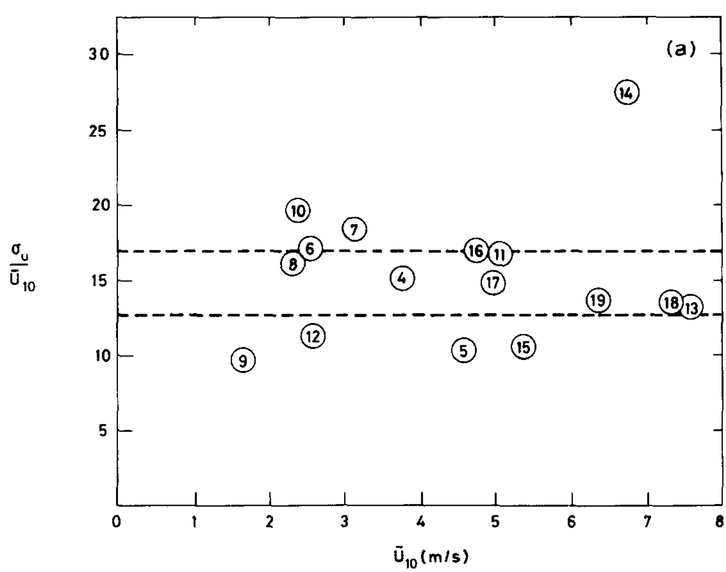

Fig. 20(a). Turbulence intensity (σ_u) at 10 m for Phase I trials (— — — ESDU data).

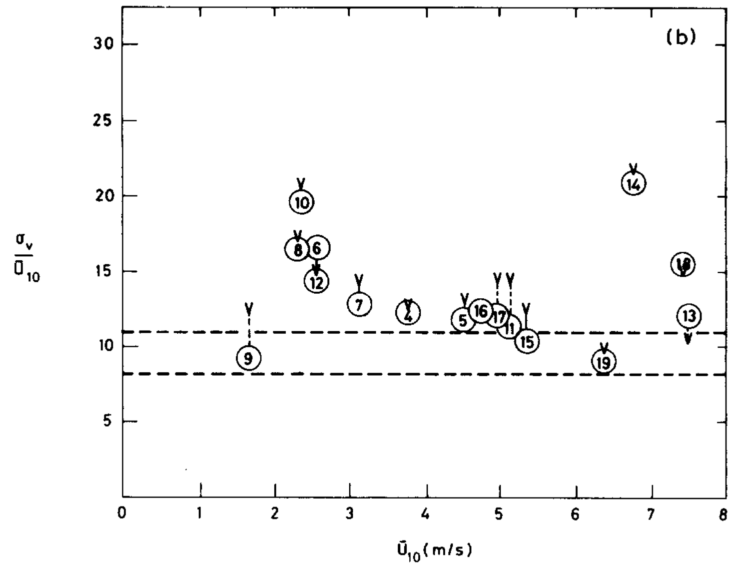

Fig. 20(b). Turbulence intensity (σ_v) at 10 m for Phase I trials (V from wind vane, ——— ESDU data).

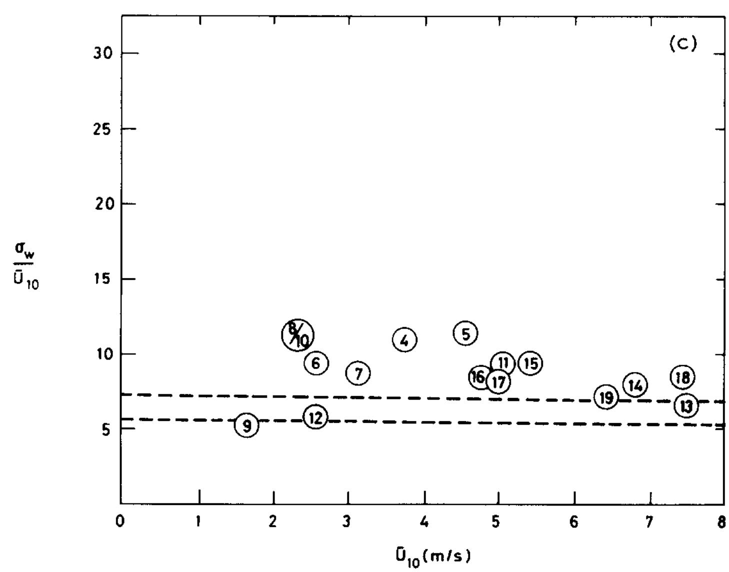

Fig. 20(c) Turbulence intensity (σ_w) at 10 m for Phase I trials (——— ESDU data).

Whilst for many applications the numerical value of turbulence intensity is important, in this paper the aim is to refine the selection of the stability descriptions given above.

5.2 Temperature profiles

Figure 21 shows the temperature profiles for the four trials under consideration presented as deviations from the 2 m temperature. The general pattern is one of decreasing stability from Trial 009 through 013 and 006 to 004 (compare with Fig. 17).

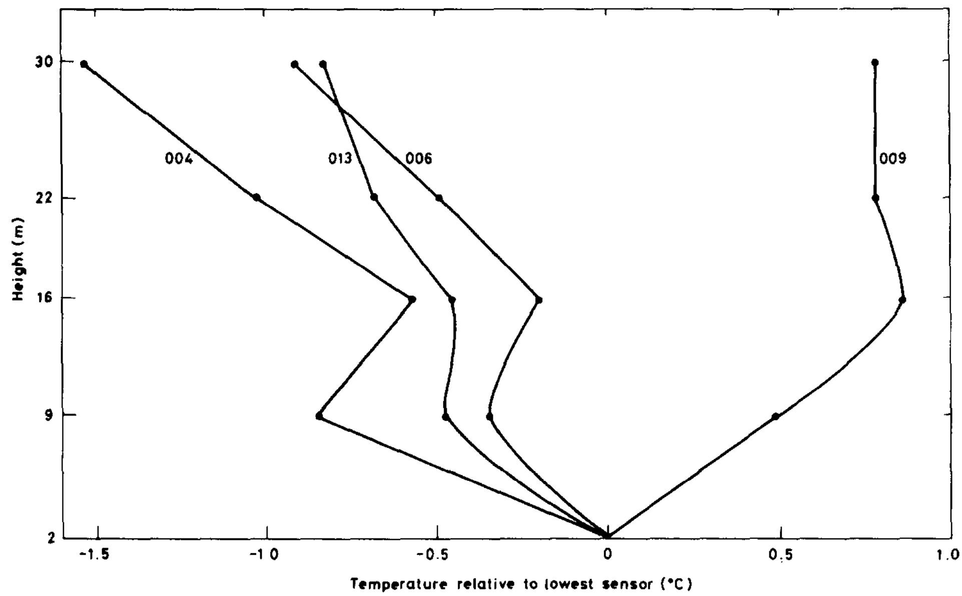

Fig. 21. Temperature profiles for selected trials.

Following the temperature gradient criteria outlined in Section 4.2.4 the stability categories which may be inferred from Fig. 21 (9 m to 30 m) are E, C, A, A respectively. Clearly, however, calculations of temperature gradient based on other portions of the profile could lead to significantly different results. Of particular interest are the "knees" in the profiles around 9 m and 16 m. Questions regarding the accuracy of the measurements remain to be addressed in more depth (the basic information on calibration is presented in Johnson [24]) but some checks on the form of the profiles can be made. In Fig. 22 further temperature distributions are shown for this purpose. Curve 1 derives from the same neutral stability condition used in Fig. 12 to provide velocity profile data in high winds (U_{10} = 13.3 m/s). The band delimited by the broken lines contains Pasquill D-stability temperature gradients. Within acceptable limits the measured profile falls in the band though some hints of profile inflexions exist.

The data plotted as curve 2 was taken during Trial 016, a low speed (4.8 m/s) reasonably neutral case with a wind direction as shown in Fig. 13. The shape is similar to that from Trial 013 (Fig. 21) though the wind heading was significantly different.

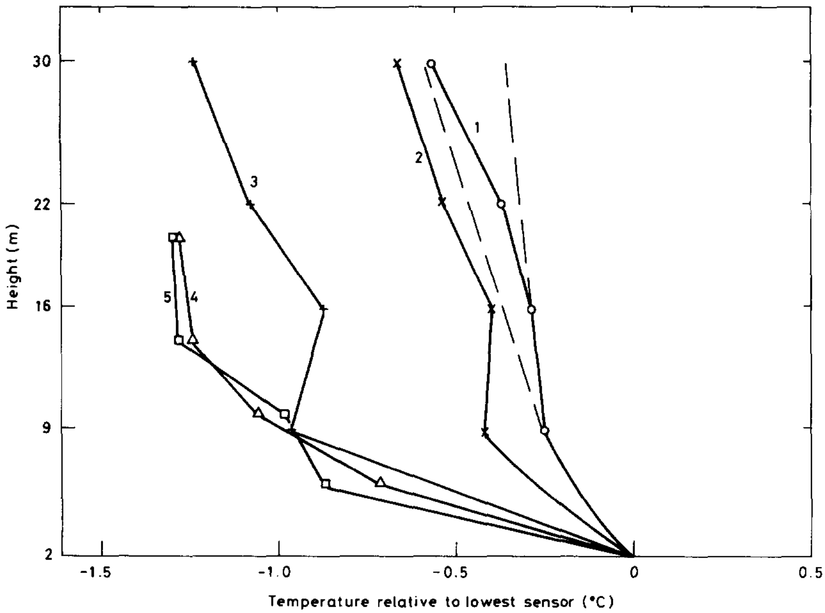

Fig. 22. Additional temperature profiles (Section 5.2).

Curve 3 is produced for comparison with Trial 004 (Fig. 21). The wind speeds were similar (around 4 m/s) but whereas in Trial 004 the wind blew just to the right of the array centre-line, on this occasion the heading was —98° (anticlockwise relative to C/L). Suspicions that the "kneed" profile may have been due to thermal plumes from upwind runway surfaces would seem to be largely discredited by this comparison. To complete the picture profiles 4 and 5 were taken from 1984 data where measurements were made with a revised system on a 20 m mast. These similar unstable profiles resulted from very different conditions

profile 4: 2.1 m/s at 22° to the array centre-line
profile 5: 6.5 m/s at 122° to the array centre-line.

From the data examined to date it would appear unlikely that the temperature inflexions were real. Basically, the 16 m sensor gave high readings and there is some evidence that this continued when the same thermometer was used at 10 m in the 1984 experiments. Although no great accuracy can be claimed for the calculation, the use of the temperature difference between 9 m and 30 m at Thorney Island as a plausible estimate of temperature gradient is generally supported by this discussion.

5.3 Velocity profile

Ming et al. [26] describe the atmospheric boundary layer wind profile as

$\bar{u}/u_* = (1/k)[\ln(z/z_0) - \psi_m(z/L)]$

where k is von Karman's constant and ψ_m is the similarity function for momentum defined as

$\psi_m = \ln[(1+\chi^2)/2((1+\chi)^2/2)] \quad -2\tan^{-1}\chi + \pi/2$

where $\chi = (1 - 16z/L)^{-0.25}$ for an unstable atmosphere, and $\psi_m = 5z/L$ for a stable atmosphere.

The resulting profile variation is shown in Fig. 23, where Golder's [13] values of L (Fig. 16) and a roughness length z_0 of 5 mm have been used. The profiles from Trials 004, 006, 009 and 013 are drawn in Fig. 24. Trials 006 and 013 fall together just on the unstable side of neutral whilst Trial 004 had a clearly unstable characteristic. The profile from Trial 009 is more complex with the appearance of a stable lower portion and an unstable upper part.

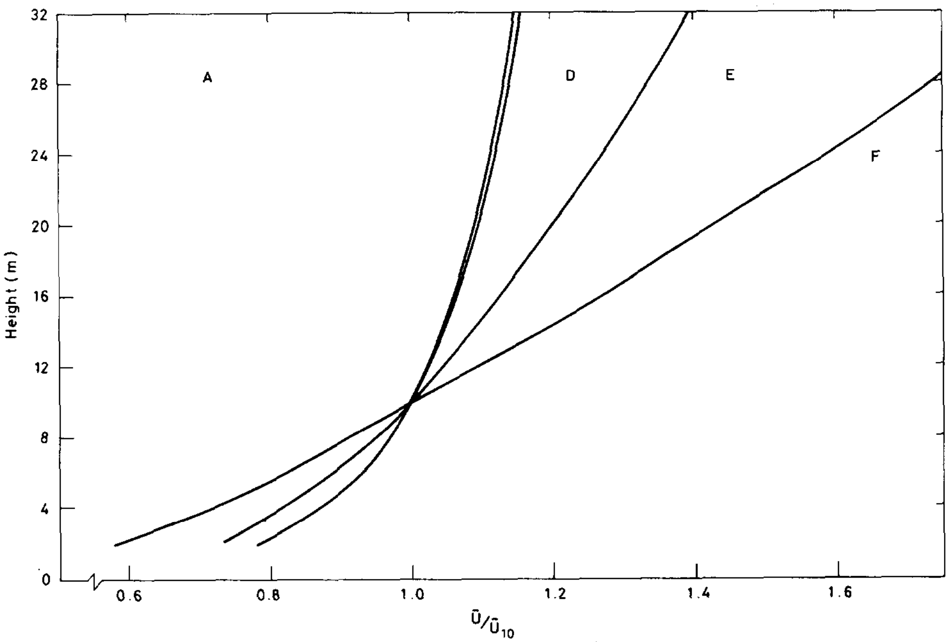

Fig. 23. Velocity profiles in varying atmospheric stability.

5.4 Trial 013

Trial 013 took place on an October morning in a wind of 7.5 m/s. The day was sunny and the prevailing conditions had developed from a stable early morning atmosphere. Table 5 summarises the stability classification indicators derived using the methods of Section 4.2. With the exception of σ_θ all indications are that the atmospheric stability was to the slightly

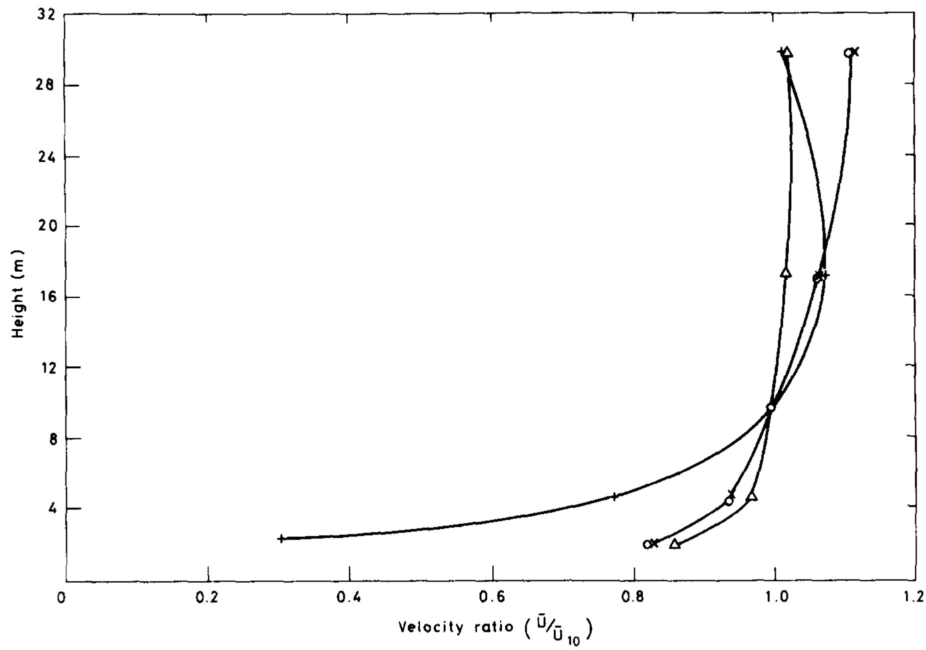

Fig. 24. Velocity profiles from selected trials (△, 004; ×, 006; +, 009; ○, 013).

unstable side of neutral. This judgement is entirely to be expected and is in reasonable accord with the Pasquill categorisation in Table 3.

5.5 Trial 006

The trial took place at the end of a summer's day in low winds. Earlier unstable conditions were gradually giving way to stable evening conditions. In cooling conditions the temperature gradient had begun to reduce in the lowest 16 m but the 9 m to 30 m gradient remained at an unstable level. As shown in Table 5 the turbulence levels at 10 m were consistently higher than in Trial 013 but the velocity profile had developed an identical form. The low insolation and resulting heat flux level reflect the trend toward increased stability. Though the various heat flux estimates are not widely different they fall in a sensitive area and suggest stability in the range of very stable to slightly unstable.

The judgement of neutral stability for this trial is an attempt to categorise the region of the boundary layer relevant to the dispersing heavy cloud. This assessment is similar to the Pasquill (Table 5) assumption of neutral conditions for higher elevations in the final hour before sunset.

5.6 Trial 009

This release was at a similar time of day to Trial 006 but on a mid-September evening, rather closer to sunset. The wind was light and turbulence levels were low. As shown in Figs. 21 and 24 the lowest 10 to 16 m exhibited stable characteristics whilst the higher levels retained an unstable appearance. In essence the conditions were a further development on 006 and the stability indicators (Table 5) describe a stable atmosphere over the depth of the released cloud.

TABLE 5

Stability indicators

Trial	013	006	009	004
Date	19/10/82	4/8/82	15/9/82	15/7/82
Time	11:41	19:11	18:45	12:28
U_{10} (m/s)	7.5	2.6	1.7	3.8
% Turbulence intensities				
σ_u/U_{10}	13.4 (neutral)	16.9 (neutral/ unstable)	9.6 (stable)	15.1 (neutral)
σ_v/U_{10}	12.0 (neutral/ unstable)	16.3 (unstable)	9.1 (neutral)	12.1 (unstable)
σ_w/U_{10}	6.4 (neutral)	9.2 (unstable)	4.9 (stable)	10.9 (unstable)
Velocity profile	slightly unstable	slightly unstable	stable (lower)	unstable
dT/dz (°C/100 m)	−1.6(C)	−2.7(A)	1.2(E)	−3.3(A)
Insolation (W/m²)	407(C)	31(E)	12(G)	452(C)
H_1 (W/m²) (Sect. 4.2.3)	123(C)	−28(G)	−35(G)	141(C)
H_2 (W/m²) uncorr. (4.2.3)	56(C/D)	11(D)	−2(D)	71(C)
H_2 (W/m²) corr. (4.2.3)	64(C/D)	11(D)	−2(D)	72(C)
H_3 (W/m²) (Sect. 4.2.3)	178(C)	18(D)	12(D)	140(C)
H_4 (W/m²) (Sect. 4.2.3)	55(D)	−29(G)	−40(G)	66(C)
μ (on H_1 to H_4)	−12(D) to −38(C)	47 (stable) to −29(C)	166 (stable) to −50(B)	−65(B) to −141(A)
L (m) (on H_1 to H_4)	−129(D) to −41(C)	12(F) to −18(C)	2(G) to −6(A)	−5(A) to −11(B)
Ri (Sect. 4.2.5)	0.109(D)	−2.097(A)	435(F)	−31.7(A)
Ri_B (Sect. 4.2.6)	−0.001(D)	−0.018(A)	0.063(F)	−0.014(A)
σ_θ vane (°) (Sect. 4.2.7)	6.0(E)	8.5(D)	7.0(E)	7.0(E)
σ_θ sonic (°) (Sect. 4.2.7)	6.9(E)	9.3(D)	5.2(E)	6.9(E)
Judged stability	C/D	D	E/F	B

The low friction velocity led to small Monin—Obukhov lengths and significant values of the Kazanski—Monin parameter in spite of small heat flux estimates. As the heat flux estimates spanned upward and downward transport a particularly large range of stability classification could be deduced from L and μ.

The final judgement of E/F is, of course, inconsistent with Table 3 which excludes stable categories in daylight. It is apparent, however, that for winds up to 5 kts (2.5 m/s) this standard scheme quickly moves into E/F classes beyond sunset.

5.7 Trial 004

Trial 004 took place around mid-day on a moderately sunny mid-July day. Table 3 would suggest a B/C stability category and this is generally the inference from the Table 5 indicators. One and a half hours before the release the boundary layer had generally similar characteristics. The turbulence levels were greater than the slightly unstable Trial 013, and there is some evidence that the cross-wind fluctuations develop rather slowly through the day. From the trials in Table 5, σ_v tends to exhibit more "history" than the other components. The heat flux measurements produced "highly unstable" values of μ and L and an overall judgement of a B category is reasonably well supported by the evidence. Once again, however, the NRC limits on the standard deviation of wind heading look suspect.

6. Conclusions

A large number of successful heavy gas dispersion trials were conducted from the Summer of 1982 to the Summer of 1984. The suitability of the site and its weather conditions were a major factor in the exercise and this paper has briefly described some of the pre- and post-project considerations made of the site characteristics and its meteorology.

The historical background meteorological data and the surface elevation measurements allowed an objective assessment of the spill and measurement array locations to be made and provided a rational basis on which to mount the operational plan.

During the trial, full recordings of the environmental sensor channels were made and in this paper sample analyses and derived parameters have been presented.

It has been shown that the site was aerodynamically relatively smooth. An appearance of roughness length dependence with wind speed has been hard to avoid but in view of the difficulty of ensuring the existence of neutrally stable conditions (Section 5) arguably only the highest wind speed estimates should be utilised. For practical purposes z_0 can be considered to be between 5 mm and 10 mm.

A number of methods have been used to judge atmospheric stability classes. Whilst wide variations can be produced by the different schemes it has been shown for the examples given here, that physically meaningful explanations can be found for the discrepancies produced. Uncertainty was greatest soon after the beginning and towards the end of daylight hours when the rate of change of stability was greatest. At these times particularly more insight into the physics of heavy gas cloud dispersion is necessary to focus the assessment on the dominant characteristics of the atmosphere for that particular spill (type and size).

Though the appeal of a single parameter classification of atmospheric stability remains great, the analysis presented has merely served to confirm the commonly held belief that complex atmospheric flows are not always amenable to such a simple description.

References

1 J. McQuaid, Objectives and design of the Phase I Heavy Gas Dispersion Trials, J. Hazardous Materials, 11 (1985) 1—33.
2 D.R. Johnson, Thorney Island trials: systems development and operational procedures, J. Hazardous Materials, 11 (1985) 35—64.
3 M.J. Leck and D.J. Lowe, Development and performance of the gas sensor system, J. Hazardous Materials, 11 (1985) 65—89.
4 H. Tennekes and J. Lumley, A First Course in Turbulence, The MIT Press, Cambridge, MA, 1972.
5 H. Tennekes, The logarithmic wind profile, J. Atmos. Sci., 30(2) (March 1973) 234—238.
6 J. Lumley and H. Panofsky, The Structure of Atmospheric Turbulence, Interscience, New York, 1964.
7 F.B. Smith, Turbulence in the atmospheric boundary layer, Sci. Prog. Oxf., 62 (1975) 127—151.
8 J.S. Puttock and G.W. Colenbrander, Thorney Island data and dispersion modelling, J. Hazardous Materials, 11 (1985) 381—397.
9 ESDU Data Sheet 74031, Characteristics of atmospheric turbulence near the ground — Part II. Single point data for strong winds (neutral atmosphere), Engineering Sciences Data Unit, London, 1974.
10 A.J. Watts, Sea breeze at Thorney Island, Meteor. Mag., 84 (992) (February 1985) 42—48.
11 F. Pasquill, Atmospheric Diffusion, Ellis Horwood, Chichester, 2nd edn., 1974.
12 G.F. Hoffnagle, M.E. Smith, T.V. Crawford and T.J. Lockhart, On-site meteorological instrumentation requirements to characterise diffusion from point sources — a workshop, 15—17 January 1980, Raleigh, N.C., Bull. Amer. Meteor. Soc., 62(2) (February 1981) 255—261.
13 D. Golder, Relations among stability parameters in the surface layer, Bound. Layer Meteor., 13(1) (September 1972) 47—58.
14 US Nuclear Regulatory Commission, On site meteorological programs, Regulatory Guide 1.23.
15 F.B. Smith, The relation between Pasquill stability and Kazanski—Monin stability (in neutral and unstable conditions), Atmos. Environ., 13 (1979) 879—881.
16 L. Sedefian and E. Bennett, A comparison of turbulence classification schemes, Atmos. Environ., 14 (1980) 741—750.
17 M. Tagliazucca and T. Nanni, An atmospheric diffusion classification scheme based on the Kazanski—Monin stability parameter, Atmos. Environ., 17(11) (1983) 2205—2211.

18 C.J. Readings, F.B. Smith and G.J. Jenkins, The heavy gas trials at Thorney Island — a review of meteorological aspects, Report by the Meteorological Office to HSE, 1982 (D/MET 0 14/5/13).
19 J.C. Kaimal, Measurements of momentum and heat flux variations in the surface boundary layer, Radio Science, 4(12) (1969) 1147—1153.
20 W. Jiemin, Estimation of fluxes from routine meteorological data, Met. Office Report TDN 153, 1984.
21 W. Jiemin, A comparison of several methods of assessing the surface energy balance over a grass surface, Met. Office Report TDN 155, 1984.
22 A. Holstag and A.P. van Ulden, A simple scheme for daytime estimates of the surface fluxes from routine weather data, KNMI Report WR 83-14, 1983.
23 H.A.R. de Bruin and A.A.M. Holstag, A simple parameterization of surface fluxes of sensible and latent heat during daytime compared with the Penman—Monteith concept, J. Appl. Meteor., 21(11) (1982) 1610—1621.
24 D.R. Johnson, Assessment of the performance of the environmental sensors during the Thorney Island trials, NMI Report, to be published (1985).
25 A.J. Dyer, A review of flux-profile relationships, Bound. Layer Meteor., 7 (1974) 363—372.
26 Z. Ming, H.A. Panofsky and R. Ball, Wind profiles over complex terrain, Bound. Layer Meteor., 25 (1983) 221—228.